Dalton Transactions

Accepted Manuscript

ROYAL SOCIETY OF CHEMISTRY

www.rsc.org/dalton

Dalton Transactions

RSCPublishing

ARTICLE

Supramolecular Control of Monooxygenase Reactivity in a Copper(II) Cryptate

Cite this: DOI: 10.1039/xoxxoooooox

L. Chaloner[a], A. Khomutovskaya[a], F. Thomas[b] and X. Ottenwaelder*[a]

Received 03rd February2016,
Accepted 00th January 2016

DOI: 10.1039/xoxxoooooox

www.rsc.org/

We report a detailed investigation of the formation and self-decomposition of Cu(II)-hydroperoxo intermediates under the influence of second-coordination-sphere features provided by a cryptand. In solution, an equilibrium between two copper complexes with square-planar and square-pyramidal geometries was identified. Upon addition of H_2O_2/Et_3N, two copper(II)-hydroperoxo intermediates formed at different rates. Their decomposition via self-oxidation was probed by deuterating select positions on the cryptand. This led to a small kinetic isotope effect of 1.5. Mass spectrometry analysis of the demetallated organic products is consistent with a direct oxygen-atom transfer to a tertiary amine on the cryptand, forming an *N*-oxide, unlike other models of copper mononuclear monooxygenase enzymes.

Introduction

In contrast to energy-consuming or hazardous industrial processes,[1-3] biological systems serve as an inspiration to develop synthetic oxidative transformations such as oxygen-atom transfers (OAT) and C–H bond hydroxylations.[4] Mechanistically, OATs are characterized by the direct transfer of an oxygen atom from a donor to an acceptor molecule while C–H bond hydroxylations generally entail a hydrogen-atom abstraction/transfer (HAT) followed by an oxygen or hydroxyl group transfer.[5,6] While developing a general synthetic procedure for OAT or C–H bond hydroxylation under mild, efficient and selective conditions is a challenge,[3] several enzymes can selectively perform this reaction using dioxygen (O_2) as the oxidant and forming water as a by-product.[2,7] For this reason, bio-inorganic chemists strive to understand and mimic biological systems to inspire synthetic oxidative transformations.[8,9] Development in this field can be achieved by understanding the nature and reactivity of the metal-O_2 intermediates in biological systems.[4]

In this paper, we focus on copper (Cu) oxidative chemistry in relation to mononuclear Cu-dependent enzymes such as peptidylglycine-α-hydroxylating monooxygenase (PHM), dopamine-β-monooxygenase (DβM) and tyramine-β-monooxygenase (TβM).[7,10] PHM catalyzes the C–H bond hydroxylation of a glycine-extended peptide to form peptidyl-α-hydroxyglycine, DβM catalyzes the hydroxylation of dopamine to form norepinephrine and TβM hydroxylates tyramine, forming octopamine.[11] These enzymes bear similar structures composed of two domains each containing a single Cu center. In PHM, and by extension in the other analogous enzymes, O_2 is activated at a mononuclear Cu(I) active site. The rate-determining step (RDS) is typically a HAT from the substrate, which is then followed by a fast transfer of the oxygen group. While Cu(II)-superoxo and Cu(II)-hydroperoxo species are involved in the enzymatic mechanism, it is now widely accepted that the Cu(II)-superoxo intermediate is the actual hydrogen abstractor.[7,11] Nevertheless, many synthetic complexes show the viability of the Cu(II)-hydroperoxo species as a HAT or OAT agent.[12-18]

The structure and reactivity of Cu/O_2 intermediates are largely determined by the ligand system.[19,20] For example, TMG_3Tren is a ligand that uses steric and electronic effects to stabilize a Cu(II)-superoxo species at low temperatures (Chart S1, A).[21] The TMG_3Tren-Cu(II)-superoxo does not oxygenate the ligand upon thermal decomposition, yet the TMG_3Tren-Cu(II)-hydroperoxo is able perform C–H bond hydroxylation on the ligand.[12] A second study shows that by using a well-tailored N_2O_2 ligand system (Chart S1, B), a thermally stable Cu(II)-hydroperoxo complex is involved in the catalysis of benzylic C–H bond oxidation of toluene and *o*-xylene.[15] In this example, DFT shows that the Cu(II)-hydroperoxo intermediate is stabilized through hydrogen bonding of the Cu(II)-hydroperoxo hydrogen to a phenolate group of the ligand. This is in contrast with BPPACu(II)(OOH) (Chart S1, C), where the hydroperoxo group is stabilized by hydrogen bonding of the proximal oxygen to the pivalamide group.[22] Taken together, these examples illustrate that the second coordination sphere of the metal centre can influence the reactivity of Cu/O_2 intermediates.

Cryptands can influence the geometry and reactivity of metals centres, imparting new behaviours on old coordinating moieties.[23-26] In previous work, we reported a Cu(II) cryptate, $[LCu(OAc)(MeOH)]^+$, based on a tris(2-aminoethyl)amine (Tren) cordinating moiety (Scheme 1).[27] The geometry of the Cu(II) centre is enforced by the cryptand to be square-pyramidal, unlike typical Tren-based complexes that adopt trigonal-bipyramidal geometries.[28,29] When the Cu(II) cryptate was reacted with hydrogen peroxide (H_2O_2) in the presence of triethylamine (Et_3N), a Cu(II)-hydroperoxo intermediate was formed. We here present a detailed analysis of its reactivity, which constitutes an extensive investigation into the influence of the second coordination sphere of a cryptand on the OAT behaviour of a Cu(II)-hydroperoxo intermediate.

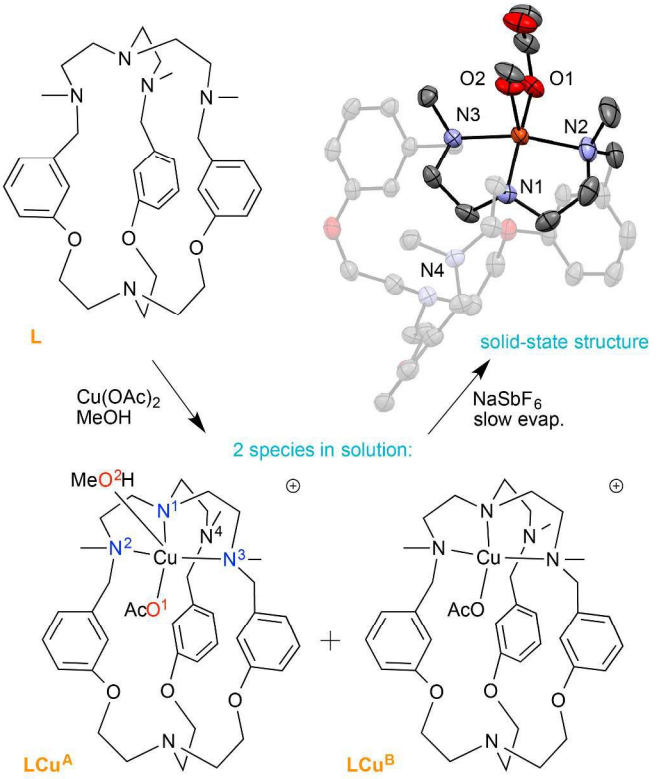

Scheme 1. Synthesis of $[LCu(OAc)(MeOH)_n]^+$ (n= 0 or 1) and its crystal structure (as a SbF_6^- salt) showcasing the geometry of the metal center.[27] Crystal: ORTEP representation at 50% thermal ellipsoid probability. The hydrogen atoms and SbF_6^- counterion have been removed for clarity.

Results and Analysis

Synthesis and Characterization of the Copper(II) complexes

The reaction of L with Cu(II) acetate leads to the formation of cryptand-Cu(II) complexes with different speciation in solution. We prepared the complexes in four ways, using two solvents and two preparation methods (see experimental section). Solutions I and II are in methanol, while solutions III and IV are in less polar dichloromethane. A solvent effect is observed (below), but at parity of solvent no significant difference is observed between solutions prepared by mixing L and Cu(II) in situ (solutions I and III) or by redissolving crystals of the pure complex (solutions II and IV).

Two Cu complexes, LCu^A and LCu^B, were identified by EPR spectroscopy on frozen solutions I-IV (Figure 1 and Figure S1). The spectra are best fitted by considering a mixture of two mononuclear Cu(II) complexes with $d(x^2\text{-}y^2)^1$ ground states ($g_\parallel > g_\perp$), with the spin Hamiltonian parameters obtained from simulation listed in Table 1.[30] Thus, the Cu(II) geometry in LCu^A and LCu^B is similar to that in the crystal structure of $[LCu(OAc)(MeOH)]^+$.[27] Although the perpendicular regions are satisfactorily fitted using the parameters given in Table 1, we refrain from commenting on the values due to the significant overlap of the signals which results in large uncertainty. Addison et al. proposed that $g_\parallel/A_\parallel$ ratio reflects the metal ion geometry, with values as low as 120 representing a square-planar geometry of the metal centre.[31] The $g_\parallel/A_\parallel$ ratios calculated for all the species (Table 1) fall within the range 124-130, *i.e.* close to 120, indicating that the tetragonal distortions are small in both species and that the metal ion geometry is not significantly different between them.

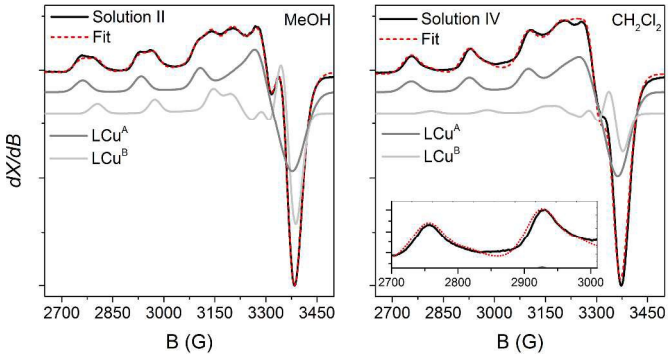

Figure 1. X-Band EPR spectra of solutions II and IV in black, Easyspin fit spectra in red and deconvolution of the fit spectra in grey.[30]

Table 1. EPR spectral parameters for solutions I-IV

Cond.	Complex	$g_\perp$ [1] ($A_\perp$ (G))[1]	$g_\parallel$ ($A_\parallel$ (G))	$g_\parallel / A_\parallel$ [2] (cm)	A:B (%)
I: in situ / MeOH	LCu^A	2.037 (22)	2.235 (189)	126	60
	LCu^B	2.056 (37)	2.216 (181)	131	40
II: crystals / MeOH	LCu^A	2.040 (17)	2.232 (188)	127	61
	LCu^B	2.047 (41)	2.204 (183)	129	39
III: in situ / CH_2Cl_2	LCu^A	2.059 (17)	2.244 (185)	130	89
	LCu^B	2.059 (44)	2.209 (176)	134	11
IV: crystals / CH_2Cl_2	LCu^A	2.052 (20)	2.238 (188)	127	83
	LCu^B	2.054 (43)	2.204 (178)	132	17

[1] Significant overlap in this region creates an uncertainty in these values.
[2] A is in cm^{-1}.

The distinguishing feature between LCu^A and LCu^B in solution is assigned to the presence or absence of a methanol molecule at the axial coordination site. The prevalent complex in solutions I-IV, LCu^A (Table 1), is proposed to retain a MeOH molecule in the axial position, similar to the solid-state structure. This assignment is supported by EPR data calculated via DFT methods (Table 2 and Supporting information). Thus, electronic optimization of a 5-coordinated $[LCu(OAc)(MeOH)]^+$ species led to $g_{\|calc}$ = 2.172. By comparison, removing the methanol and optimizing the structure led to a $[LCu(\eta^2\text{-}OAc)]^+$ species with a bidentate acetate ion. This species is calculated to have a smaller $g_{\|calc}$ = 2.163, as does LCu^B, and a higher distortion (as indicated by its larger $g_\| / A_\|$ parameter), as does LCu^B. Thus, we propose that LCu^A is $[LCu(OAc)(MeOH)]^+$ and LCu^B is $[LCu(OAc)]^+$ (Scheme 1; see Figure S8 for further analysis of coordinating anions).

Table 2. DFT-calculated EPR and structural parameters for various LCu and LCuOOH models.

Species [1]	[g] g1 g2 g3	[A] (MHz) A1 A2 A3	g_3/A_3 (cm)	τ
$[LCu(\eta^2\text{-}OAc)]^+$	2.033 2.070 2.163	-49 -242 -836	77.54	0.266
$[LCu(OAc)_{eq}(MeOH)_{ax}]^+$	2.041 2.064 2.172	-108 -229 -878	74.12	0.093 [2]
$[LCu(OOH)_{eq}]^+$	2.033 2.044 2.132	-124 -219 -790	80.87	0.038
$[LCu(OOH)_{eq}(MeOH)_{ax}]^+$ [3]	2.034 2.047 2.139	-120 -223 -809	79.24	0.076
$[LCu(OOH)_{eq}(OAc)_{ax}]$	2.024 2.080 2.152	-125 -194 -622	103.70	0.109
$[LCu(OAc)_{eq}(OOH)_{ax}]$ [4]	2.037 2.072 2.175	-134 -249 -782	83.33	0.625

[1] ax = axial, eq = equatorial. [2] The τ parameter for the X-ray structure is 0.104. [3] The MeOH is effectively dissociated (Cu···O = 3.188 Å). [4] This species is energetically less stable than its $[LCu(OOH)_{eq}(OAc)_{ax}]$ isomer.

Formation and EPR Analysis of the Copper(II)-Hydroperoxo Intermediates and their Decomposition Products

Reaction of the $LCu^{A/B}$ solution with a H_2O_2/Et_3N solution in methanol leads to a colour change from blue to green to yellow-green. This progression, shown in Scheme 2, was followed at low temperatures with different spectroscopic and spectrometric techniques as described below.

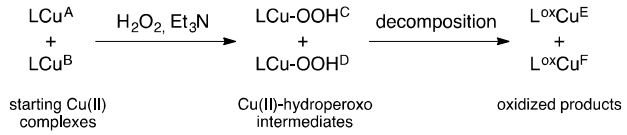

Scheme 2. Summary of reaction and products

The EPR spectrum recorded after mixing solution I with 20 equiv. H_2O_2/Et_3N at -90°C for 1 min does not exhibit any signal attributable to the initial compound LCu^A and LCu^B, consistent with full consumption of the starting material (Figure 2). The EPR spectrum is composed of two signals typical for square-based Cu(II) mononuclear complexes ($g_\| > g_\perp$, $d(x^2\text{-}y^2)^1$ ground state), indicating that again two species were present in solution, LCu-OOH^C and LCu-OOH^D (Figure 2 and Table 3). The $g_\|/A_\|$ ratios for LCu-OOH^C and LCu-OOH^D (136 and 148 cm respectively) are higher than for the starting complexes, revealing that the Cu(II) geometry evolved upon formation of the hydroperoxo intermediates, with LCu-OOH^D displaying the highest tetragonal distortion. DFT computation of several LCuOOH species was performed to help identify the intermediates (Table 2). The lowest-energy state for $[LCu(OOH)_{eq}(MeOH)_{ax}]^+$ has the methanol decoordinated to give $[LCuOOH]^+$, which is the species with the smallest $g_\|$ among those calculated. Between the two isomers $[LCu(OOH)_{eq}(OAc)_{ax}]$ and $[LCu(OAc)_{eq}(OOH)_{ax}]$, the former was found logically to be more energetically stable. By comparison of the experimental and calculated EPR parameters we suggest that LCu-OOH^C and LCu-OOH^D are $[LCu(OOH)_{eq}(OAc)_{ax}]$ and $[LCuOOH]^+$, respectively.

The square-based Cu(II) geometry in LCu-OOH^C and LCu-OOH^D contrasts with the trigonal-bipyramidal Cu(II) geometry found in Me_6TrenCuOOH (Chart S1, D, Me_6Tren = tris(2-(*N*,*N*-dimethylamino)ethyl)amine), which has a similar ligand donor set to L.[29] This demonstrates that restraining the coordinating arms within a cryptand structure has a dramatic impact on the geometry on the Cu(II) species, and therefore on their reactivity (below).

Analysis of the solutions obtained after complexes LCu-OOH^C and LCu-OOH^D decompose informs on the oxidative pathway(s) undergone by the Cu(II)-hydroperoxo intermediates. The EPR spectrum of the decomposition products mainly consists of an axial Cu(II) signal with $g_\| > g_\perp$ ($L^{ox}Cu^E$), but introduction of a second component with $g_\perp > g_\|$ ($L^{ox}Cu^F$, $d(z^2)^1$-like ground state) in ca. 16% was required to improve the fit significantly (Table 3). The major complex, $L^{ox}Cu^E$, displays a $g_\|/A_\|$ ratio of 129 cm, and thus has a similar Cu(II) geometry as in the initial complexes LCu^A and LCu^B. The $g_\perp$ and $A_\perp$ values of this minor complex, $L^{ox}Cu^F$, are indicative of a trigonal-bipyramidal Cu(II) geometry.[32]

Table 3. EPR spectral parameters for solution I + H_2O_2/Et_3N

Conditions	Complex	$g_\perp$ [1] ($A_\perp$ (G))[1]	$g_\parallel$ ($A_\parallel$ (G))	$g_\parallel / A_\parallel$ [2] (cm)	C:D or E:F (%)
I + H_2O_2/ Et_3N	LCu-OOH^C	2.037 (32)	2.235 (174)	136	76
	LCu-OOH^D	2.063 (31)	2.200 (158)	148	24
Decomposition	L^{ox}Cu^E	2.055 (14)	2.251 (186)	129	84
	L^{ox}Cu^F	2.178 (68)	2.017 (71)	306	16

[1] Significant overlap in this region creates an uncertainty in these values.
[2] A is in cm^{-1}

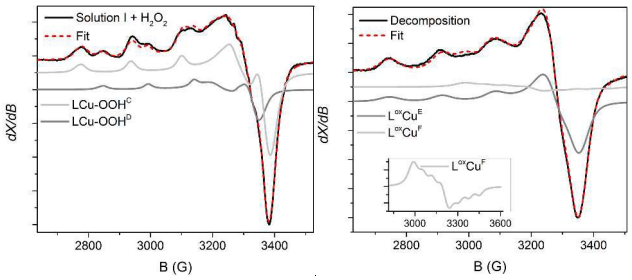

Figure 2. X-Band EPR spectra of Solution I + 50 equiv. H_2O_2/Et_3N and decomposition product

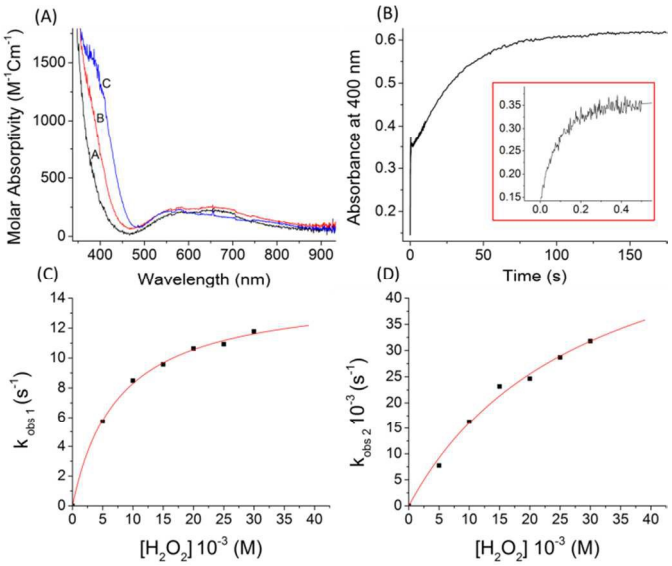

Figure 3. Top: Spectral data of the reaction of solution I (0.5 mM) and 10 equiv. Et_3N + 40 equiv. H_2O_2 at -50 °C in MeOH. (A) UV/Vis spectra at A: 2.5 ms B: 0.875 s and C: 174.87 s. (B) Time profile of absorbance at 400 nm. Inset: zoom from 0 to 0.55 s. (C) and (D): Observed pseudo first order rate constants of the reaction of Solution I in the presence of 10 equiv. Et_3N + 10-60 equiv. H_2O_2 at -50 °C vs $[H_2O_2]$. (C) fast process and (D) slow process. The red trace indicates a fit to $k_{obs} = kK[H_2O_2][Et_3N] / (1 + K[Et_3N])$ where, $K_1 = 133$ and $k_1 = 2902\ s^{-1}$ for graph (C) and $K_2 = 14$ and $k_2 = 24\ s^{-1}$ for graph (D).

Kinetic Analysis

Formation of the Hydroperoxo Intermediates

Formation of two Cu(II)-hydroperoxo intermediates is confirmed by low-temperature stopped-flow UV/Vis spectroscopy. In addition to a slow-forming LMCT absorption band at 388 nm ($\varepsilon \approx 2000\ M^{-1}cm^{-1}$), previously identified,[27] a fast process with a λ_{max} of 375 nm was detected at -50°C (Figure 3). Significant spectral changes in the visible region, corresponding to d-d transitions, occur only upon the slow process, reflecting a greater change in geometry for the slower-forming complex (Figure S9). We therefore assign the LMCT at 388 nm (slow process) to the complex with a greater tetragonal distortion, LCu-OOH^D.

The rate constants of both the fast and slow processes are $[H_2O_2]$-dependent and obey saturation kinetics (Figure 3, A and B). Fitting the saturation behavior with Itoh's model that involves a $[H_2O_2] + [Et_3N] \rightleftharpoons [HOO^-\cdot Et_3NH^+]$ pre-equilibrium, where $[HOO^-\cdot Et_3NH^+]$ reacts with the complex to form the hydroperoxo intermediate,[33] led to different equilibrium constants for the fast ($K_1 = 133$) and slow ($K_2 = 14$) processes. The discrepancy indicates that the fast and slow reactions cannot be fitted to the same model and suggests that two different mechanistic pathways are operative. Despite our best attempts, the rate constants could not be extracted from the data, presumably due to the additional $[LCu^A] + [MeOH] \rightleftharpoons [LCu^B]$ equilibrium.

Decomposition of the Hydroperoxo Intermediates

The decomposition of the slow-forming intermediate was analysed with stopped-flow UV/Vis at 20°C by monitoring the decay of the absorption at 388 nm. Solution I, in the presence of 10 equiv. Et_3N in methanol, was mixed with 10-40 equiv. H_2O_2 and the resulting UV/Vis trace of the reaction was fitted to a first-order model. Statistics were used to probe the rate of decomposition for dependence on $[H_2O_2]$.[34] One-factor ANOVA showed that varying the concentration of H_2O_2 from 20 to 40 equiv. resulted in statistically similar means ($F_{2,12} = 0.072$, $p > 0.05$) (see Note S1 for further details). The rate of decomposition was therefore considered to be independent of $[H_2O_2]$ (Figure 4).

To gain further insight into the decomposition of the LCu-OOH$^{C/D}$ mixture, we synthesized cryptand L^D with 15 deuterium atoms substituting for hydrogen atoms at the most oxidatively sensitive C–H bonds, namely the methyl groups and the benzylic positions (Scheme 3). ESI-MS analysis shows that 87% of the product had incorporated all 15 deuterium atoms (see experimental section). The Cu(II) complexes with L^D and their subsequent oxidation reactions were examined under the same conditions as with L. On one hand, no kinetic isotope effect (KIE = k_H/k_D) was observed for the formation of the Cu(II)-hydroperoxo intermediate along the slower process. On the other hand, the decomposition reaction, analyzed at several H_2O_2 concentrations, exhibited a KIE that was averaged to be 1.5 ± 0.1 (Figure 4, Table S1). This value is much lower than the one measured in DβH ($k_H/k_D = 10.6$).[35]

Few KIEs have been reported for the decomposition of synthetic Cu(II)-hydroperoxo intermediates. A KIE of 2.3 was measured in a case of oxidative *N*-demethylation that is proposed to proceed via rate-limiting C–H abstraction.[18] Alternatively, *N*-debenzylation on a very similar system proceeds through site-specific Fenton chemistry with a KIE of 1.0.[36] Aromatic C–H bond hydroxylation via a Cu(II)-alkylperoxo intermediate exhibited an inverse KIE of 0.9, consistent with a rate-limiting electrophilic aromatic substitution.[16] In our case, the low magnitude of the KIE indicates a small influence of the aliphatic C–H bonds on the rate-determining step of the Cu(II)-hydroperoxo oxidative decomposition.

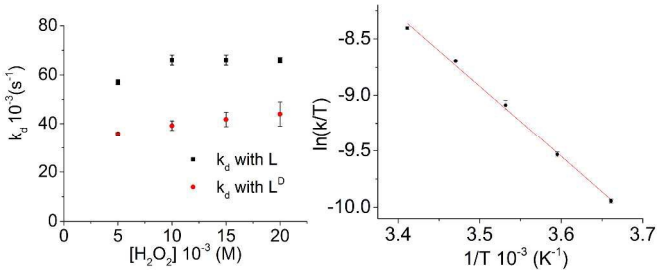

Figure 4. Left: Plot of the first order rate of decomposition of (black) $[LCuOOH]^+$ and (red) $[L^DCuOOH]^+$ versus $[H_2O_2]$ Average KIE was 1.5 ± 0.1. Right: Eyring plot for the first-order rate constants of decomposition measured at 0, 5, 10, 15 and 20 °C: 1.29 x 10^{-2}, 2.01 x 10^{-2}, 3.20 x 10^{-2}, 4.23 x 10^{-2}, 6.59 x 10^{-2} s^{-1}, respectively (standard deviation from fitting within 1.1 to 6.9 %).

Table 4. Activation parameters for intramolecular decomposition and natural decay pathways.

Intermediate	Decomposition Reaction	$\Delta H^{\ddagger}$ (kJ mol^{-1})	$\Delta S^{\ddagger}$ (J K^{-1} mol^{-1})	ref
Bis(μ-oxo), Peroxo[1]	Intramolecular *N*-dealkylation	52 to 63	–23 to –100	37
Bis(μ-oxo), Peroxo[1]	Intramolecular benzylic hydroxylation	28 to 42	–62 to –155	37
CuOOH[2]	Natural decay	43	–119	38
CuOOR[3]	Intramolecular aromatic hydroxylation	24	–162	16
CuOOH[4]	Intramolecular *N*-oxygenation	51	–94	This work

[1]Several ligand systems used, [2]*N*,*N*-bis(2-pyridylmethyl)bis(2-pyridyl)methylamine), [3]*N*,*N*-di(2-pyridylmethyl)benzylamine, [4]L

The Eyring activation parameters for decomposition of the $LCu\text{-}OOH^{C/D}$ solution are $\Delta H^{\ddagger}$ = 51 kJ mol^{-1} and $\Delta S^{\ddagger}$ = –94 J K^{-1} mol^{-1} (Figure 4). The parameters are similar to those reported for the decomposition of Cu(II)-OOR (R = H or alkyl) and intramolecular C–H bond hydroxylation with bis(μ-oxo)dicopper(III) and peroxodicopper(II) species (Table 4).[16,37,38] The negative sign of $\Delta S^{\ddagger}$ suggests that the transition state is constrained, consistent with the suggested intramolecular decomposition pathway. The magnitude of the $\Delta S^{\ddagger}$ suggests significant structural changes during decomposition, consistent with EPR data showing a decrease in Cu geometric distortion in the decomposition product $L^{ox}Cu^{E}$ compared with hydroperoxo intermediates $LCu\text{-}OOH^{C/D}$. Alternatively, a solvent molecule (MeOH) or anion may be associating to the complex upon decomposition. $\Delta S^{\ddagger}$ is,

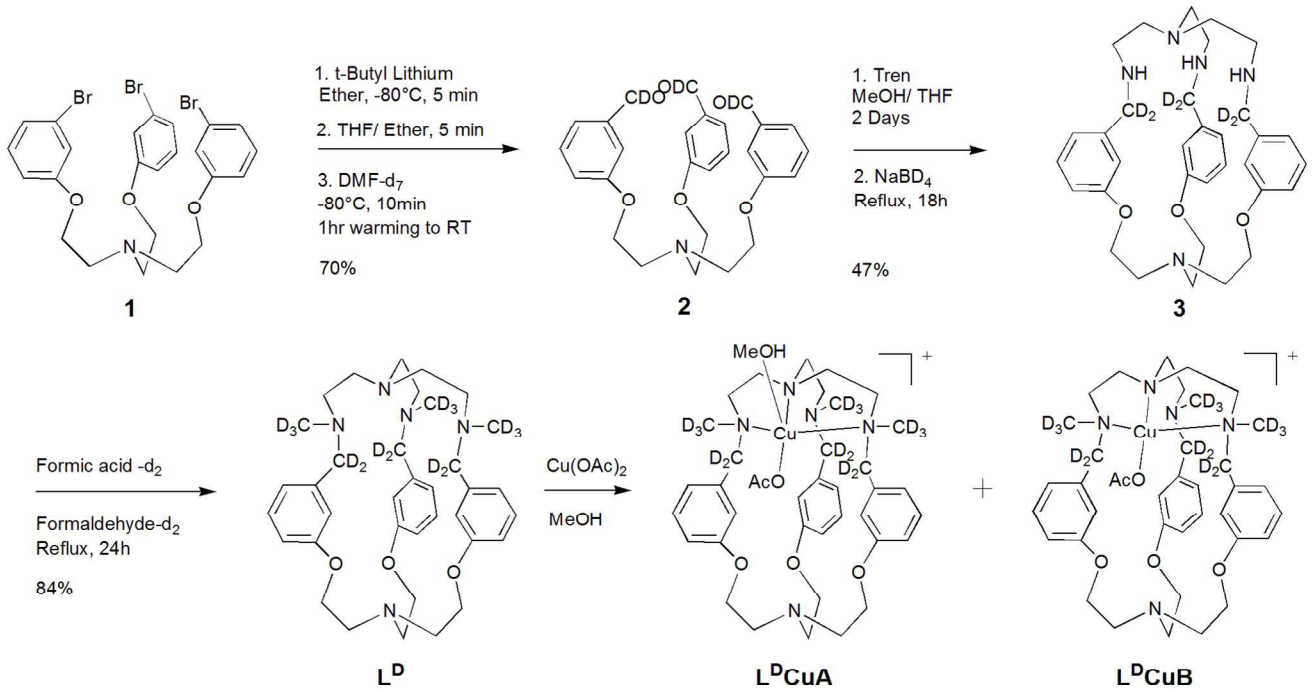

Scheme 3. Synthesis of the L^D and its copper(II) acetate complexes L^DCu^A and L^DCu^B.

however, less negative than for the decomposition of other Cu(II)–OOH/OOR species,[37] highlighting a significant degree of preorganization in the cryptand-based complexes.

Analysis of the Oxidation Products

Intramolecular oxidation on a macrocycle or a cryptand offers a unique perspective on the reactivity of Cu/O_2 intermediates in that the products of oxidation remain tethered to the scaffold. CSI-MS was used to monitor the oxidation in a similar manner to our previous ESI-MS procedure.[27] The softer CSI ionization technique and lower temperature resulted in cleaner spectra with fewer ions from side-reactions and/or fragments (Figure 5). The spectra (A to D) were dominated by the peaks for $[LCuOAc]^+$ and $[(L+O)CuOAc]^+$. In spectrum B, the peak at m/z = 697.3264 was found within 0.7 ppm of the exact mass of the formula $C_{36}H_{52}N_5O_5Cu$, which could represent either $[LCuOOH]^+$ or $[(L+O)CuOH]^+$, the latter being more likely given the time and temperature of mixing before injection. Over time, the signal for the monooxygenated complex (m/z = 739) increased in intensity (Figure 5, B to D). Minimal over-oxidation was observed. Using $H_2{}^{18}O_2$ exclusively generates the $[(L+{}^{18}O)CuOAc]^+$ complex, proving that the extra oxygen atom in $L^{ox}Cu^{E/F}$ indeed comes from H_2O_2 and therefore from $LCu\text{-}OOH^{C/D}$.[27]

The CSI-MS experiment using deuterated ligand, L^D, provided some of the most telling data in terms of reactivity (Figure 5, E). The m/z peaks seen in the reaction of both $[LCuOAc]^+$ and $[L^DCuOAc]^+$ differ by the number of deuterium atoms (15 units). This suggests that both sets of complexes react in a similar fashion and that ligand deuteration does not affect the reaction pathway. Importantly, the major oxygenated product retains all of the deuterium atoms throughout the course of the reaction, indicating that all C–D bonds remain intact during the major reaction pathway. This finding contradicts the previously proposed mechanism where the distal OH of the coordinated hydroperoxo unit abstracts a deuterium atom from the benzylic position of the ligand and leaves as a water molecule (Scheme S1). In this case, the final oxygenated product would have exchanged a deuterium for a hydrogen atom.[27]

Demetallation of the decomposed solutions confirms that the extra oxygen atom is incorporated in the ligand and further informs on the nature of the oxidation reaction. Demetallation with NH_4OH resulted in a mass recovery greater than 90 %. The organic products were identified by ESI-MS as the starting ligand (L), ligand with one additional oxygen atom (L+O) and a very small amount of over-oxidized product (L+2O-2H) (Figure 6). When using L^D, all 15 deuterium atoms are conserved in the oxygenated product (L^D+O), confirming that all C–D bonds are intact after oxidation (Figure 6). ^{1}H-NMR spectra show only a small amount of an aldehyde signal, indicating that the major product of the reaction, L+O, is not an aldehyde as originally proposed (Scheme S1).[27] In our previous report, we used $EDTA_{(aq)}$ to demetallate the complex and extracted the organic matter into dichloromethane. This procedure, however, results in less than 5% mass recovery, and the products recovered are the starting ligand (L) and the over-oxidized product (L+2O-2H) (Figure S10, B). A strong signal at 9.92 ppm in the ^{1}H-NMR spectrum of this solution signifies that the aldehyde we previously reported is actually the over-oxidized product and not L+O. In addition, the major change in the ^{1}H-NMR upon D/H substitution of the ligand is the disappearance of the aldehyde signal in the deuterated sample, indicating that over-oxidation likely occurs at a benzylic position.

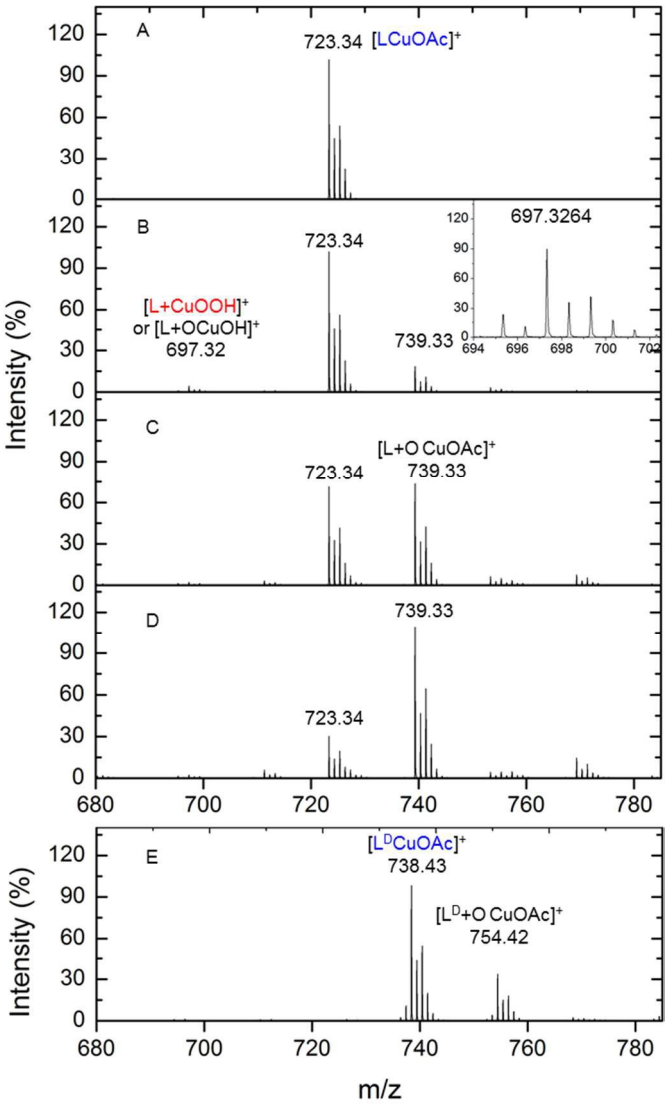

Figure 5. CSI-MS of solution I and 5 equiv. H_2O_2/Et_3N mixed with a continuous-flow method at RT. The spectra were recorded with L at (A) 0 s, (B) 60 s with inset showing zoom of 697, (C) 270 s and (D) 540 s and with L^D at (E) 270 s.

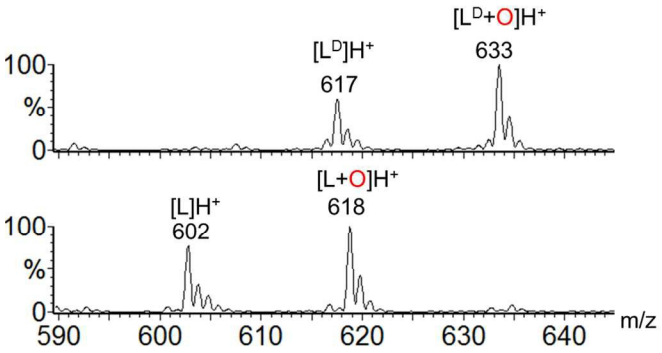

Figure 6. ESI-MS of the organic products after reaction with 5 equiv. H_2O_2/Et_3N and demetallation with NH_4OH. Top: L^D; bottom: L.

Discussion

Formation of an N-Oxide

The analysis of EPR, stopped-flow UV/Vis and mass spectrometry, using both the deuterated and non-deuterated cryptands leads us to propose the formation of a mixture of two hydroperoxo intermediates that decompose via an OAT reaction and not the hypothesized C–H bond abstraction pathway.

The mechanism for the formation of the hydroperoxo intermediates is complex and warrants speculation. It is likely that the two starting Cu(II) species, LCu^A and LCu^B, undergo separate fast and slow reactions, in parallel, to form the two hydroperoxo intermediates. This is supported by the fact that the EPR spectra of the intermediates show two new complexes in solution during acquisition, and both fast and slow rates of formation are dependent on $[H_2O_2]$. Although a sequential mechanism involving $LCu\text{-}OOH^C \rightarrow LCu\text{-}OOH^D$ cannot be ruled out, the evidence argues in favour of two parallel reactions.

Common intramolecular decomposition pathways for Cu(II)-hydroperoxo intermediates are *N*-dealkylation, benzylic hydroxylation and aromatic hydroxylation, all of which involve oxidation at a C–H bond.[12,13,16-18,36,39] While these intramolecular reaction pathways are conceivable with $LCu\text{-}OOH^{C/D}$, the analysis (^{1}H-NMR, IR, MS) of the self-oxidation reaction suggests another pathway, namely through a nucleophilic attack of the uncoordinated tertiary amine (N4) of Tren on the Cu-OOH moiety, causing cleavage of the OOH moiety and formation of an *N*-oxide (Scheme 4). The most compelling piece of evidence is the MS data that shows conservation of ligand structure and all deuterium atoms after the self-oxidation. If oxidation at a C–H bond had occurred, at least one deuterium atom would be replaced by a hydrogen atom upon work-up or demethylation would have been observed at m/z = 588. This is illustrated in Scheme S1 via the formation a hemiaminal function (iii), and rearrangement to an aldehyde and amine as the major products (iv). The insignificant amount of an aldehyde signal in the ^{1}H-NMR spectrum confirms that this was not the major reaction pathway.

While OAT reactions from an *N*-oxide to a metal centre are typical,[40] metal-promoted formation of an aliphatic *N*-oxide on a ligand, as seen in $L^{ox}Cu^{E/F}$ (L^{ox} = L+O), is quite rare.[41] The two examples, involving Cu(I)/O_2[42] and Fe(III)/*t*BuOOH[43] reactions, suggest that *N*-oxide formation in our case occurs on the uncoordinated tertiary amine of the cryptand. Unfortunately, we were unable to isolate a pure sample of L+O for further analysis of the N–O stretch by IR, due to decomposition of the sample upon chromatography.

Control experiments confirm the inner-sphere nature of the OAT. It is known that H_2O_2 can react with tertiary amines to yield *N*-oxides (outer sphere pathway), but the yields are usually low.[41] In our case, addition of 5 equivalents of H_2O_2/Et_3N to L in DCM/MeOH resulted in less than 5% oxidation of the ligand. At this stage, it is unknown whether the mechanism involves a direct OAT to the aliphatic amine or a site-specific Fenton-like pathway, as reported recently.[36] In the latter case, the release of radical intermediates would likely target the C–H(D) bonds. We therefore advocate for the direct OAT pathway from $LCu\text{-}OOH^{C/D}$, whereby the small KIE can be explained as a secondary isotope effect and suggests that the OAT takes place in the vicinity of the C–H(D) bonds.

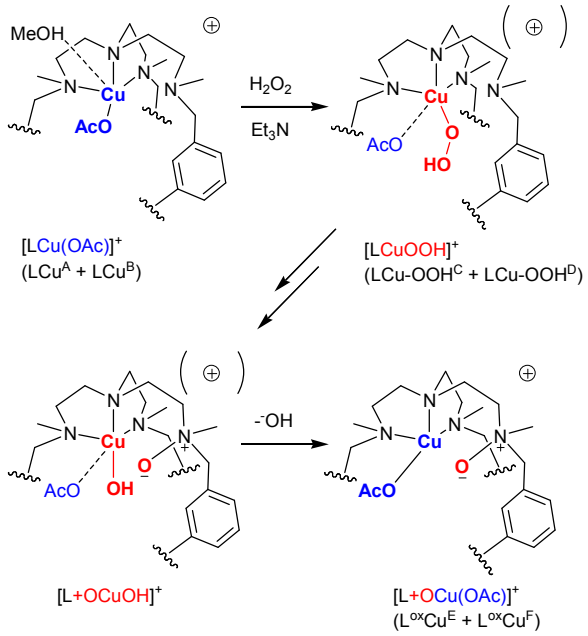

Scheme 4. Proposed mechanism for the decomposition of the hydroperoxo intermediates.

Second Coordination Sphere Effects

The supramolecular/rigid nature of the ligand has a pronounced effect on the reactivity of the Cu(II)-hydroperoxo species. *N*-methylation imposes additional constraints in cryptands and prevent metal centres from adopting C_3 symmetry.[44] The geometries of LCu^A and LCu^B were identified as square-pyramidal and square-planar, respectively. In comparison, copper(II) complexes of Me_6Tren, a ligand with the same donor set but free from the restrictions of macrocycles, are trigonal-

bipyramidal in solution.[28,29,45] Masuda et al. proposed that the reactivity of a hydroperoxo intermediate is greatly influenced by the geometry of the metal centre; specifically that square-planar complexes have higher reactivity than trigonal-bipyramidal complexes.[14] With the Me_6Tren ligand, the Cu(II)-hydroperoxo undergoes neither intra- nor inter-molecular oxidations,[29] whereas Cu(II)-hydroperoxo complexes of the L cryptand do show intramolecular reactivity. The difference can be explained in part by the rigidity of the cryptand enforcing the more reactive geometry.

L has five tertiary amines available, yet the major product of the reaction is a singly oxygenated amine. There are several examples of copper complexes with ligands bearing tertiary amines that have been reacted with H_2O_2 in the presence of a base and have preferentially undergone C–H bond oxidation rather than formation of *N*-oxides.[12,17,18] The major difference between these ligands and cryptand L is the steric constraint that the cryptand enforces, likely positioning the uncoordinated tertiary amine for reactivity. The involvement of C–H bonds in the OAT, observed as the small KIE, is a testament to the degree of control. Thus, by enforcing the geometry of the metal centre and positioning of the site of oxidation, the cryptand controls the reactivity of the hydroperoxo intermediate through second coordination sphere features.

Conclusions

The goal of the research was to explore the second coordination sphere effects of a coordinating cryptand on the reactivity of a hydroperoxo intermediate. In this context, the formation and decomposition of a hydroperoxo intermediate have been studied. Two copper complexes were identified in solution and when reacted with hydrogen peroxide formed two hydroperoxo intermediates. The intermediates decomposed into one major copper complex. A deuterated cryptand was used to evaluate the decomposition pathway and help decipher the mechanism. It was found that upon decomposition and demetallation, there was no loss of deuterium atoms despite oxidation of the ligand. This evaluation led to an uncommon decomposition pathway for a Cu(II)-hydroperoxo intermediate, whereby an *N*-oxide was formed instead of C–H bond oxidation products. Mononuclear metallo-enzymes create protective pockets to specifically position the metal, oxidant and substrate to react cohesively. Although this level of control is currently out of reach in model systems, the present study shows that the semi-rigidity of cryptands can be used to control the reactivity of a mononuclear centre towards oxygen-atom transfer rather than hydrogen abstraction.

Experimental

Materials

All materials were used as received from Alfa Aesar and Sigma Aldrich. NMR spectroscopic measurements were made at 22 °C in a 5 mm tube on a Varian Innova 300 or 500 MHz instrument and referenced to internal tetramethylsilane. Electrospray ionization mass-spectrometry (ESI-MS) measurements were performed via direct injection on a Micromass Quattro LC or Micromass Q-TOF at Concordia's Centre for Biological Applications of Mass Spectrometry. Cryospray ionization MS (CSI-MS) data were acquired with a Bruker CSI Q-TOF at the Université de Montréal. The m/z data reported are based on ^{1}H, ^{12}C, ^{14}N, ^{16}O, and ^{63}Cu.

Synthesis of 1: Tris[2-(3-bromobenzene)-oxo]ethyl]amine

This synthesis was adapted from literature procedures.[46,47] To a solution of 3-bromophenol (1.52 g, 14.4 mmol) in 1-propanol (100 mL) was added crushed NaOH (0.6 g, 15 mmol). Solid tris(2-chloroethyl)amine (1 g, 4.8 mmol) was added to the solution. The reaction was heated at 110 °C for 4 h. After cooling, H_2O (50 mL) was added and the organic products were extracted with CH_2Cl_2 (3 x 30 mL). The combined extracts were concentrated under reduced pressure. The product was purified by flash chromatography with solid loading and a 40 g silica ReadiSep Gold column on an automated Combiflash (Teledyne Isco). The product was eluted with CH_2Cl_2 and the by-products were eluted with gradient from 0 to 100 % MeOH. The first fraction was collected and the solvent was removed under reduced pressure to afford 1.35 g (75 %) of a colourless oil. ^{1}H-NMR (500 MHz, $CDCl_3$): δ = 3.12 (t, 6H, J = 5, CH_2), 4.057 (t, 6H, J = 5, CH_2), 6.79 (m, 3H, Ar_2), 7.02 (m, 3H, Ar), 7.06 (m, 3H, Ar), 7.11 (m, 3H, Ar) ppm.

Synthesis of 2: Tris[2-(3-benzaldehyde-α-d_1)oxo]ethyl]amine

This reaction was carried out under inert conditions (nitrogen atmosphere, dry solvents). To a Schlenk flask containing distilled tetramethylethylenediamine (2.21 mL, 14.79 mmol) in diethyl ether (50 mL) was added **1** (1.345 g, 2.1 mmol). After cooling the solution to -78 °C, *t*BuLi (8.7 mL of a 1.7 M in pentane, 14.79 mmol) was cautiously added. The reaction was stirred for 10 minutes with a yellow precipitate forming. THF (15 mL) was added to the solution, which was stirred for an additional 5 min. DMF-d_7 (1.2 mL, 15.75 mmol) was then added and the reaction was allowed to warm to RT at which stage it was opened to the air. $NH_4Cl_{(sat)}$ (30 mL) was added and the organic products were extracted with CH_2Cl_2 (3 x 20 mL). The combined extracts were concentrated under reduced pressure. The product was purified with column chromatography using EtOAc/Hexane gradient elution from 20/80 to 50/50 on silica. The third fraction was collected and the solvent was removed under reduced pressure to afford 696 mg (71 %) of a colourless oil. ^{1}H-NMR (500 MHz, $CDCl_3$): δ = 3.2 (t, 6H, J = 6, CH_2), 4.15 (t, 6H, J = 6, CH_2), 7.12 (m, 3H, Ar_2), 7.35 (m, 3H, Ar), 7.42 (s, 3H, Ar), 7.45 (m, 3H, Ar) ppm.

Synthesis of 3

The following procedure was adapted from previously published work.[46] To a vigorously stirring solution of **2** (696 mg, 1.5 mmol) in 500 mL THF:MeOH (1:10) was added tris(2-aminoethyl)amine (220 µL, 1.5 mmol) in 50 mL methanol via syringe pump over 5 hours. The reaction was left to stir at 25 °C for 48 h. The solvent was reduced to 50 mL and $NaBD_4$ (313

mg, 7.5 mmol) was added slowly. The reaction was stirred at 25 °C for 30 min then refluxed for 48 h. The solvent was removed under reduced pressure. The resulting precipitate was washed with acetonitrile and dried under vacuum to give 400 mg (47 %) of a white powder. ^{1}H-NMR (500 MHz, $CDCl_3$): δ = 1.51 (s, 3H, NH), 2.58 (m, 12H, CH_2), 3.02 (t, 6H, J = 5, CH_2), 3.96 (t, 6H, J = 5, CH_2), 6.48 (s, 3H, Ar), 6.705 (m, 3H, Ar), 6.855 (m, 3H, Ar), 7.14 (m, 3H, Ar) ppm. ^{13}C-NMR (500 MHz, $CDCl_3$): δ 47.86 (CH_2), 55.78 (CH_2), 56.22 (CH_2), 67.77 (CH_2), 77.21 (CH_2), 112.85 (Ar), 114.36 (Ar), 120.48 (Ar), 128.98 (Ar), 142.09 (Ar), 159.42 (Ar). The signal-to-noise ratio was too low to see the ^{13}C signal of the CD_2 groups.

Synthesis of L^D

Formic acid-d_2 (429 µL, 8.5 mmol) and formaldehyde-d_2 (1.336 mL, 8.5 mmol) were added to **3** (400 mg, 708 µmol). The solution was refluxed for 24 h, then cooled and poured onto chilled aqueous NaOH (30 mL, 2 M). The product was extracted with dichloromethane (3 x 20 mL) and the organic phase extracts were dried with anhydrous Na_2SO_4. The solvent was removed under reduced pressure, yielding a precipitate that was suspended in acetonitrile. Filtration, washing with acetonitrile and drying under vacuum afforded 370 mg (84 %) of a white crystalline powder. A suitable crystal for X-ray crystallography was chosen and shows same unit cell as **L**: *a* 13.2, *b* 13.5, *c* 18.5 [Å], α 90, β 90, γ 90 [°].[27] ^{1}H-NMR (500 MHz, $CDCl_3$): δ = 2.33 (t, 6H, J = 7, CH_2), 2.60 (t, 6H, J = 7, CH_2), 3.06 (t, 6H, J = 6, CH_2), 4.02 (t, 6H, J = 7, H_2), 6.68 (m, 3H, Ar), 6.755 (m, 3H, Ar), 7.05 (s, 3H, Ar), 7.11 (m, 3H, Ar) ppm. ^{13}C-NMR (500 MHz, $CDCl_3$): δ 52.26 (CH_2), 54.12 (CH_2), 57.23 (CH_2), 68.75 (CH_2), 114.50 (Ar), 114.56 (Ar), 121.36 (Ar), 128.77 (Ar), 140.64 (Ar), 159.23 (Ar). The signal-to-noise ratio was too low to see the ^{13}C signal of the CD_2 and CD_3 groups. MS (ESI, 1:1 CH_3OH:CH_2Cl_2): *m/z* = 617 (87 % incorporation of 15 D), 616 (9 % incorporation of 14 D), 615 (3 % incorporation of 13 D) $[M+H]^+$.

Synthesis of L and [LCu(OAc)(MeOH)](SbF$_6$)

The syntheses of L and [LCu(OAc)(MeOH)](SbF_6) were previously reported.[27] An alternative crystallization method is described here: to solution I (see below) was added 1 equiv. of solid $KSbF_6$ (9.20 mg, 50 µmol) or $NaSbF_6$. The solution was stirred for 20 min and then left to slowly evaporate over 48 h to give dark blue crystals. The crystals were washed with cold methanol and air-dried to give 37 mg of [LCu(OAc)(MeOH)](SbF_6), 73 % yield.

Synthesis of [LCu(OAc)](OAc) and [LCu(OAc)(MeOH)](OAc)

Solution I: To L (30 mg, 50 µmol) dissolved in 200 µL of dichloromethane was added $Cu(OAc)_2 \cdot H_2O$ (10 mg, 50 µmol) dissolved in 800 µL of methanol. After 5 minutes of stirring, the solvent was removed under reduced pressure and 1 mL of methanol was added to dissolve the complex. The final volume of methanol was varied depending on the desired concentration.

Solution II: Crystals of [LCu(OAc)(MeOH)](SbF_6) (10 mg, 10 µmol) were added to methanol and stirred with reflux with for 0.5 h. The volume of methanol was varied depending on desired concentration.

Solution III: To L (30 mg, 50 µmol) dissolved in 1 mL of dichloromethane was added $Cu(OAc)_2 \cdot H_2O$ (10 mg, 50 µmol). The solution was stirred for 4 h and then used as is. The final volume of dichloromethane was varied depending on the desired concentration.

Solution IV: Crystals of [LCu(OAc)(MeOH)](SbF_6) (10 mg, 10 µmol) were added to dichloromethane and stirred for 10 min. The volume of dichloromethane was varied depending on desired concentration.

Synthesis of [L^DCu(OAc)](OAc), [L^DCu(OAc)(MeOH)](OAc) and [L^DCu(OAc)(MeOH)](SbF_6)

To L^D (31 mg, 50 µmol) dissolved in 200 µL of dichloromethane was added $Cu(OAc)_2 \cdot H_2O$ (10 mg, 50 µmol) dissolved in 800 µL of methanol. The complex could be crystallized with 1 equialent of $KSbF_6$ followed by slow evaporation.[27] The procedure for solution I-IV was used to prepare the sample. Formation was evidenced by a single ESI-MS signal: accurate mass = 738.4334, exact mass = 738.43569, mass accuracy = 3.1 ppm.

EPR Measurements

X-band EPR spectra were collected on a Bruker EMX Plus spectrometer controlled with Xenon software and equipped with a Bruker teslameter. A Bruker nitrogen-flow cryostat connected to a high-sensitivity resonant cavity was used for 100 K measurements. Samples of 400 µL of 0.5 mM solutions were frozen in liquid nitrogen. The spectra were fit with Easyspin Fitting software.[30]

DFT calculations

Theoretical calculations were performed with the ORCA program package.[48,49] Geometry optimizations was performed by using the GGA functional BP86,[50-52] with a def2-TZVP[53] basis set for all atoms. The RI approximation was used in combination with the def2-TZVP/J auxiliary basis set.[54,55] The integration grids were typically Grid4, while the SCF convergence criterion was set to TightSCF in the ORCA convention. The EPR properties were computed by using the hybrid functional B3LYP,[56,57] with the def2-TZVP[53] basis set. In order to optimize the computational cost the RIJCOSX approximation[58] was used, together with the def2-TZVP/J auxiliary basis set.[54,55] Larger integration grids were used, in combination with the zero-order regular approximation (ZORA)[59] and a Slowconv criterion. For the treatment of the spin orbit coupling a complete mean field approach was used, with the Coulomb terms treated via the RI.

Kinetic Measurements

Kinetic studies of the reaction of H_2O_2/Et_3N with solution I were recorded on a BioLogic low-temperature stopped-flow unit (Claix, France) equipped with a J&M TIDAS diode-array spectrophotometer (J&M, Aalen, Germany). Solutions after mixing were 0.5 mM with respect to Cu in 184 µL of methanol.

All concentrations are reported as in-cell, after dilution. The concentration of H_2O_2 was varied from 5 to 30 mM with Et_3N held at 5 mM. The reaction was studied at temperatures between 20 and -50 °C. Spectra (330-1025 nm) were collected and analyzed with a global analysis fitting routine using the program Reactlab kinetics (Jplus Consulting, Palmyra, Australia).

Oxidation Reaction with H_2O_2/Et_3N

This procedure has been previously reported.[27,33]

Demetallation Studies

WITH NH_4OH

Solution I was reacted with 5 equiv. of H_2O_2/Et_3N and allowed to decompose (heat or time). NH_4OH (2 mL) was added and the solution was filtered over alumina in a Pasteur pipet. The alumina was rinsed with MeOH (10 mL) followed by CH_2Cl_2 (20 mL). The filtrate was washed with water (3 x 10 mL) and dried over Na_2SO_4. The solvent was removed under reduced pressure. Mass recovery: 31 mg, (103 w%) of L, L+O and L+2O-2H, minor products.

WITH EDTA

Solution I was reacted with 5 equiv. of H_2O_2/Et_3N and allowed to decompose (heat or time). Solid Na_2EDTA (100 mg) was added and the solution was stirred for 5 min. The solution was then filtered over a pipet-full of alumina, which was rinsed with MeOH and CH_2Cl_2 as above. The filtrate was washed with water (3 x 10 mL) and dried over Na_2SO_4. Mass recovery: 28 mg, (93 w%) of L, L+O and L+2O-2H, minor products.

Alternatively, after the reaction of solution I with 5 equiv. of H_2O_2/Et_3N, $Na_2EDTA_{(aq)}$ (30 mL, 0.1 M) was added and the solution was left to stir for 5 min. L and the over-oxidized product were extracted with 3 x 10 mL of CH_2Cl_2, dried over Na_2SO_4 and the solvent was removed under reduced pressure. Mass recovery: 1 mg (3 w%) of L and L+2O-2H and minor products.

Acknowledgements

This work has been supported by Fonds de Recherche du Québec - Nature et les Technologies (FRQNT) and the Natural Sciences and Engineering Research Council of Canada (NSERC). L.C. acknowledges Concordia University for the Mobility Award and FRQNT for the Bourse de Stage International: Centre in Green Chemistry and Catalysis. We would like to thank Prof. Garry Hanan (Université de Montréal) for access to the CSI-MS and Dr. Jingwei Luo (Universtiy of Victoria) for training on the CSI-MS. We are grateful to Dr. Andrey Moiseev and Prof. Scott Bohle (McGill University) for preliminary EPR measurements.

Notes and references

[a] Department of Chemistry and Biochemistry, Concordia University, 7141 Sherbrooke Street West, Montreal, H4B 1R6, Canada.

[b] Équipe de Chimie Inorganique Redox, Département de Chimie Moléculaire, Université Joseph Fourier, 38041 Grenoble, Cedex 9, France.

Electronic Supplementary Information (ESI) available. See DOI: 10.1039/b000000x/

1. H. Arakawa, M. Aresta, J. N. Armor, M. A. Barteau, E. J. Beckman, A. T. Bell, J. E. Bercaw, C. Creutz, E. Dinjus, D. A. Dixon, K. Domen, D. L. DuBois, J. Eckert, E. Fujita, D. H. Gibson, W. A. Goddard, D. W. Goodman, J. Keller, G. J. Kubas, H. H. Kung, J. E. Lyons, L. E. Manzer, T. J. Marks, K. Morokuma, K. M. Nicholas, R. Periana, L. Que, J. Rostrup-Nielson, W. M. H. Sachtler, L. D. Schmidt, A. Sen, G. A. Somorjai, P. C. Stair, B. R. Stults and W. Tumas, *Chem. Rev.*, 2001, **101**, 953.

2. E. Roduner, W. Kaim, B. Sarkar, V. B. Urlacher, J. Pleiss, R. Gläser, W.-D. Einicke, G. A. Sprenger, U. Beifuß, E. Klemm, C. Liebner, H. Hieronymus, S.-F. Hsu, B. Plietker and S. Laschat, *ChemCatChem*, 2013, **5**, 82.

3. J. Wencel-Delord, T. Droge, F. Liu and F. Glorius, *Chem. Soc. Rev.*, 2011, **40**, 4740.

4. L. Que and W. B. Tolman, *Nature*, 2008, **455**, 333.

5. R. H. Holm, *Chem. Rev.*, 1987, **87**, 1401.

6. J. M. Mayer, *Acc. Chem. Res.*, 2011, **44**, 36.

7. E. I. Solomon, D. E. Heppner, E. M. Johnston, J. W. Ginsbach, J. Cirera, M. Qayyum, M. T. Kieber-Emmons, C. H. Kjaergaard, R. G. Hadt and L. Tian, *Chem. Rev.*, 2014, **114**, 3659.

8. Y. Makita, K. Sugimoto, K. Furuyoshi, K. Ikeda, S.-i. Fujiwara, T. Shin-ike and A. Ogawa, *Inorg. Chem.*, 2010, **49**, 7220.

9. S. Yamaguchi and H. Masuda, *Sci. Technol. Adv. Mater.*, 2005, **6**, 34.

10. J. P. Klinman, *Chem. Rev.*, 1996, **96**, 2541.

11. R. L. Osborne and J. P. Klinman, in *Copper-Oxygen Chemistry*, John Wiley & Sons, Inc., 2011, pp. 1.

12. D. Maiti, D.-H. Lee, K. Gaoutchenova, C. Würtele, M. C. Holthausen, A. A. Narducci Sarjeant, J. Sundermeyer, S. Schindler and K. D. Karlin, *Angew. Chem. Int. Ed.*, 2008, **47**, 82.

13. M. Mizuno, K. Honda, J. Cho, H. Furutachi, T. Tosha, T. Matsumoto, S. Fujinami, T. Kitagawa and M. Suzuki, *Angew. Chem. Int. Ed.*, 2006, **45**, 6911.

14. T. Fujii, A. Naito, S. Yamaguchi, A. Wada, Y. Funahashi, K. Jitsukawa, S. Nagatomo, T. Kitagawa and H. Masuda, *Chem. Commun.*, 2003, 2700.

15. S. Biswas, A. Dutta, M. Debnath, M. Dolai, K. K. Das and M. Ali, *Dalton Trans.*, 2013, **42**, 13210.

16. A. Kunishita, J. D. Scanlon, H. Ishimaru, K. Honda, T. Ogura, M. Suzuki, C. J. Cramer and S. Itoh, *Inorg. Chem.*, 2008, **47**, 8222.

17. D. Maiti, A. A. Narducci Sarjeant and K. D. Karlin, *Inorg. Chem.*, 2008, **47**, 8736.

18. D. Maiti, A. A. Narducci Sarjeant and K. D. Karlin, *J. Am. Chem. Soc.*, 2007, **129**, 6720.

19. M. Zhao, H.-B. Wang, L.-N. Ji and Z.-W. Mao, *Chem. Soc. Rev.*, 2013, **42**, 8360.

20. J.-N. Rebilly, B. Colasson, O. Bistri, D. Over and O. Reinaud, *Chem. Soc. Rev.*, 2015, **44**, 467.

21. C. Würtele, E. Gaoutchenova, K. Harms, M. C. Holthausen, J. Sundermeyer and S. Schindler, *Angew. Chem. Int. Ed.*, 2006, **45**, 3867.

22. A. Wada, M. Harata, K. Hasegawa, K. Jitsukawa, H. Masuda, M. Mukai, T. Kitagawa and H. Einaga, *Angew. Chem. Int. Ed.*, 1998, **37**, 798.
23. J.-N. Rebilly and O. Reinaud, in *Copper-Oxygen Chemistry*, John Wiley & Sons, Inc., 2011, pp. 321.
24. L. Fabbrizzi and A. Poggi, *Chem. Soc. Rev.*, 2013, **42**, 1681.
25. L. Chaloner and X. Ottenwaelder, *Tetrahedron Lett.*, 2013, **54**, 3363.
26. S. O. Kang, J. M. Llinares, V. W. Day and K. Bowman-James, *Chem. Soc. Rev.*, 2010, **39**, 3980.
27. L. Chaloner, M. S. Askari, A. Kutteh, S. Schindler and X. Ottenwaelder, *Eur. J. Inorg. Chem.*, 2011, 4204.
28. F. Thaler, C. D. Hubbard, F. W. Heinemann, R. van Eldik, S. Schindler, I. Fábián, A. M. Dittler-Klingemann, F. E. Hahn and C. Orvig, *Inorg. Chem.*, 1998, **37**, 4022.
29. Y. J. Choi, K.-B. Cho, M. Kubo, T. Ogura, K. D. Karlin, J. Cho and W. Nam, *Dalton Trans.*, 2011, **40**, 2234.
30. S. Stoll and A. Schweiger, *J. Magn. Reson.*, 2006, **178**, 42.
31. H. Yokoi and A. W. Addison, *Inorg. Chem.*, 1977, **16**, 1341.
32. Y. Lee, G. Y. Park, H. R. Lucas, P. L. Vajda, K. Kamaraj, M. A. Vance, A. E. Milligan, J. S. Woertink, M. A. Siegler, A. A. Narducci Sarjeant, L. N. Zakharov, A. L. Rheingold, E. I. Solomon and K. D. Karlin, *Inorg. Chem.*, 2009, **48**, 11297.
33. T. Osako, S. Nagatomo, T. Kitagawa, C. Cramer and S. Itoh, *J. Biol. Inorg. Chem.*, 2005, **10**, 581.
34. D. C. Harris, *Quantitative Chemical Analysis*, Sixth Edition edition edn., W. H. Freeman, 2002.
35. S. M. Miller and J. P. Klinman, *Biochemistry*, 1983, **22**, 3091.
36. S. Kim, J. W. Ginsbach, J. Y. Lee, R. L. Peterson, J. J. Liu, M. A. Siegler, A. A. Sarjeant, E. I. Solomon and K. D. Karlin, *J. Am. Chem. Soc.*, 2015, **137**, 2867.
37. E. A. Lewis and W. B. Tolman, *Chem. Rev.*, 2004, **104**, 1047.
38. T. Kamachi, Y.-M. Lee, T. Nishimi, J. Cho, K. Yoshizawa and W. Nam, *J. Phys. Chem. A*, 2008, **112**, 13102.
39. D. Maiti, H. R. Lucas, A. A. N. Sarjeant and K. D. Karlin, *J. Am. Chem. Soc.*, 2007, **129**, 6998.
40. S. Hong, A. K. Gupta and W. B. Tolman, *Inorg. Chem.*, 2009, **48**, 6323.
41. D. Bellus, S. R. Chemler, D. Enders, D. Geffken, A. Köllner, W. Maison, I. O'Neil, P. Rademacher and E. Schaumann, *Science of Synthesis: Houben-Weyl Methods of Molecular Transformations Vol. 40b: Amine N-Oxides, Haloamines, Hydroxylamines and Sulfur Analogues, and Hydrazines*, Thieme, 2014.
42. C. X. Zhang, H.-C. Liang, E.-i. Kim, Q.-F. Gan, Z. Tyeklar, K.-C. Lam, A. L. Rheingold, S. Kaderli, A. D. Zuberbuhler and K. D. Karlin, *Chem. Commun.*, 2001, 631.
43. A. Nielsen, F. B. Larsen, A. D. Bond and C. J. McKenzie, *Angew. Chem. Int. Ed.*, 2006, **118**, 1602.
44. S. Derossi, D. T. Farrell, C. J. Harding, V. McKee and J. Nelson, *Dalton Trans.*, 2007, 1762.
45. R. Barbucci, A. Mastroianni and M. J. M. Campbell, *Inorg. Chim. Acta*, 1978, **27**, 109.
46. D. K. Chand and P. K. Bharadwaj, *Inorg. Chem.*, 1996, **35**, 3380.
47. K. Ziach, M. Ceborska and J. Jurczak, *Tetrahedron Lett.*, 2011, **52**, 4452.
48. F. Neese, *ORCA an ab initio, Density Functionnal and Semiempirical Program Package*, (2010) Universität Bonn, Bonn, Germany.
49. F. Neese, *Wiley Interdiscip. Rev.: Comput. Mol. Sci.* , 2012, **2**, 73.
50. J. P. Perdew, *Phys. Rev. B*, 1986, **33**, 8822.
51. J. P. Perdew, *Phys. Rev. B*, 1986, **34**, 7406.
52. A. D. Becke, *Phys. Rev. A*, 1988, **38**, 3098.
53. A. Schäfer, C. Huber and R.Ahlrichs, *J. Chem. Phys.*, 1994, **100**, 5829.
54. F. Neese, *J. Comput. Chem.*, 2003, **24**, 1740.
55. F. Weigend, *Phys. Chem. Chem. Phys.*, 2006, **8**, 1057.
56. A. D. Becke, *J. Chem. Phys.*, 1993, **98**, 5648.
57. C. Lee, W. Yang and R. G. Parr, *Phys. Rev. B*, 1988, **37**, 785.
58. F. Neese and G.Olbrich, *Chem. Phys. Lett.*, 2002, **362**, 170.
59. E. v. Lenthe, E. J. Baerends and J. G. Snijders, *J. Chem. Phys.*, 1993, **99**, 4597.